MET O 11 TECHNICAL NOTE No. 117

The parameterization of subgridscale topography

by

R. W. Riddaway

Abstract

A description is given of a simple method of parameterizing the effects of subgridscale topography. Examination of the 24 hour rainfall accumulations in a mountainous region for 12 days shows that the scheme is significently better than the operational model; there is also no significent difference between the parameterization scheme and Bell's 3½km orographic model.

Meteorological Office (MO11)
London Road,
Bracknell, Berkshire
United Kingdom.
October 1978

1. Introduction

Numerical weather prediction models usually contain an explicit representation of the topography in a highly smoothed form. However this may not be suitable for the accurate prediction of rainfall amounts. For example, a recent study by Bell (1977) (hereafter referred to as B) has shown that the 10-level model markedly underestimates the rainfall over Wales and also Wickham (1977) has found a general deficiency in rainfall over the U.K. and adjacent continental areas.

B formulated a model that could be used in conjunction with the 10-level model to predict rainfall in mountainous regions. He used information from the 10-level model to run an orographic model with a $3\frac{1}{3}$ km grid and found that this model produced a significant improvement in the 24 hr rainfall accumulations. However there was no feedback between the orographic model and the larger scale model. Also, since topography is not usually available on a $3\frac{1}{3}$ km grid, this approach cannot be used as a general method of parameterising the effects of the subgridscale topography.

White (1972) has referred to a possible parameterisation scheme based on the vertical displacement of airflow over small scale mountain elements. He also outlined a way of including the effects of different orientations of the wind relative to the topography. The scheme described in this note adopts the same kind of approach as described by White.

2. The vertical fluxes of heat and moisture

The parameterisation scheme is formulated using the same approach as is used for many deep convection schemes; examples of such schemes are given by Bates (1977) . However in the scheme described here the low level forcing is provided by topographic lifting.

Let $\bar{s}$, $\bar{r}$, $\bar{\omega}$ and $\bar{\underline{V}}$ be the grid-mean values of the dry static energy ($s+c_p\bar{T}+g\bar{Z}$), humidity mixing ratio, vertical velocity ($\frac{dP}{dt}$) and the horizontal velocity and let s', r' , ω' and $\underline{V}'$ be the departures from the mean

due to the subgridscale topography. If there is no significant correlation between the departures, then the effect of the subgridscale topography on $\bar{s}$ and $\bar{r}$ is given by

$$\frac{\partial \bar{s}}{\partial t} = L(\bar{c}-\bar{e}) - \frac{\partial}{\partial p}(\overline{s'\omega'}) \qquad (2.1)$$

$$\frac{\partial \bar{r}}{\partial t} = -(\bar{c}-\bar{e}) - \frac{\partial}{\partial p}(\overline{r'\omega'}) \qquad (2.2)$$

where $\bar{c}$ and $\bar{e}$ are the associated grid-mean values of condensation and evaporation.

The major assumption made in this parameterisation scheme is that the effects of subgridscale topography can be incorporated by introducing a single peak to the mean topography in each grid square ; the height of the peak being related to the roughness of the terrain (see figure 1). On the windward side the air is forced upwards whilst there is a compensating downdraught on the leeward side. We do not take into account that in reality the effect of the subgridscale topography will depend upon the wind direction.

Let ω_u and ω_d be the additional vertical velocities induced by the peak on the windward and leeward sides and let α be the fractional area of the ascent (with a value of 0.5). If $\hat{\omega}_u$ and $\hat{\omega}_d$ are the vertical velocities when all the topography is included (mean plus subgridscale), then

$$\hat{\omega}_u = \bar{\omega} + \omega_u \qquad \hat{\omega}_d = \bar{\omega} + \omega_d \qquad (2.3)$$

since the additional ascent must be matched by the compensating descent, we have

$$\alpha\omega_u + (1-\alpha)\omega_d = 0$$

Using this in (2.3) gives

$$\hat{\omega}_u = \bar{\omega} + \omega_u \qquad \hat{\omega}_d = \bar{\omega} - \omega_u\left(\frac{\alpha}{1-\alpha}\right) \qquad (2.4)$$

We now consider the flux of dry static energy given by

$$\overline{s'\omega'} = \overline{s\omega} - \bar{s}\,\bar{\omega}$$

$$= \alpha s_u \hat{\omega}_u + (1-\alpha) s_d \hat{\omega}_d - \bar{s}\,\bar{\omega} \qquad (2.5)$$

where s_u and s_d refer to the ascending and descending branches. Using

$$\bar{s} = \alpha s_u + (1-\alpha) s_d$$

with (2.4), we find that (2.5) becomes

$$\overline{s'\omega'} = -g M_u (s_u - s_d) \quad \text{with} \quad M_u = -\frac{\alpha \omega_u}{g} \qquad (2.6)$$

Substituting (2.6) in (2.1) yields

$$\frac{\partial \bar{s}}{\partial t} = L(\bar{c} - \bar{e}) + g \frac{\partial}{\partial p}\left\{ M_u (s_u - s_d) \right\} \qquad (2.7)$$

A similar procedure is followed for r and, if everything is expressed in terms of $\chi = Lr$ (the moist energy), we have

$$\frac{\partial \bar{\chi}}{\partial t} = -L(\bar{c} - \bar{e}) + g \frac{\partial}{\partial p}\left\{ M_u (\chi_u - \chi_d) \right\} \qquad (2.8)$$

3. The vertical flux of momentum

We use essentially the same scheme that Schneider and Lindzen (1976) used to take account of momentum transfers by convection. The relationship that corresponds to that given by (2.6) is

$$\overline{\underline{V}'\omega'} = -g M_u (\underline{V}_u - \underline{V}_d)$$

and so the effect of the momentum fluxes on $\bar{\underline{V}}$ is given by

$$\frac{\partial \bar{\underline{V}}}{\partial t} = g \frac{\partial}{\partial p}\left\{ M_u (\underline{V}_u - \underline{V}_d) \right\} \qquad (3.1)$$

with $\underline{V}_u$, $\underline{V}_d$ and $\bar{\underline{V}}$ related by

$$\bar{\underline{V}} = \alpha \underline{V}_u + (1-\alpha) \underline{V}_d$$

4. The basis of the parameterisation scheme

When air flows over an isolated hill we have some knowledge of the path a given parcel of air will take. However, this is not so for complex terrain and so in the parameterisation scheme no assumptions are made about the actual

path of the air. Instead we assume that the essential features can be parameterised by having two disconnected vertical branches to the flow; an ascending branch forced by the topography and a compensating descending branch. Therefore the effects of the subgridscale topography are taken into account by an adjustment to the flow. This procedure is similar to that used in deep convection schemes and the analogy is carried further in the treatment of the ascending branch.

In deep convection schemes it is usually assumed that the convective cells are entraining plumes with both the mass flux and vertical velocity increasing throughout most of the plume. However for the flow of statically stable air over a hill the velocity of the updraught on the windward side decreases with height. Therefore, using the analogy with the convection, we assume that the updraught is a detraining plume.

The similarity in the updraughts produced by convection and flow over hills is illustrated by considering the vertical variation of mass flux. For an entraining plume the mass flux M satisfies

$$\frac{\partial M}{\partial p} = -\gamma M$$

where γ is the entrainment rate, and if treated as a constant we have

$$\frac{\partial^2 M}{\partial p^2} = \gamma^2 M \qquad (4.1)$$

For gravity-inertial waves (wavelength 100-1000 km) the vertical velocity w induced by the topography satisfies

$$\frac{\partial}{\partial z}\left\{\left(\frac{f^2}{V^2k^2} - 1\right)\frac{\partial w}{\partial z}\right\} - l^2 w = 0 \qquad (4.2)$$

where V is the horizontal wind speed and l the Scorer parameter (for example see Eliassen (1973)). Treating the fractional area of ascent α as constant, and ignoring the vertical derivatives of $\left(f^2/V^2k^2 - 1\right)$ and ρ, (4.2) can be put in terms of the mass flux $M = \rho \alpha w$; changing from z to p coordinates this then becomes

$$\frac{\partial^2 M}{\partial p^2} = \frac{l^2}{\left(\frac{f^2}{V^2k^2} - 1\right)(\rho g)^2} M = \lambda^2 M \qquad (4.3)$$

which is similar to (4.1)

To a good approximation $\ell = \ell_0 e^{-cz}$ and $\ell = \ell_0 e^{-kz}$, and with $c \approx k$ we have

$$\lambda = \frac{\ell_0}{\ell_0 g \sqrt{\frac{F^2}{V^2 k^2} - 1}} \tag{4.4}$$

5. <u>The equations for a detraining plume</u>

The equations for a detraining plume are

$$\frac{\partial M_u}{\partial p} = \lambda M_u \tag{5.1}$$

$$\frac{\partial}{\partial p}(M_u s_u) = \lambda M_u s_u - \frac{L\bar{c}}{g} \tag{5.2}$$

$$\frac{\partial}{\partial p}(M_u \chi_u) = \lambda M_u \chi_u + \frac{L\bar{c}}{g} \tag{5.3}$$

Using these in conjunction with (2.7) and (2.8) we have

$$\frac{\partial \bar{s}}{\partial t} = g\lambda M_u (s_u - s_d) - g M_u \frac{\partial s_d}{\partial p} - L\bar{e} \tag{5.4}$$

$$\frac{\partial \bar{\chi}}{\partial t} = g\lambda M_u (\chi_u - \chi_d) - g M_u \frac{\partial \chi_d}{\partial p} + L\bar{e} \tag{5.5}$$

These are essentially the same as the equations used for parameterising the effects of deep convection, and can be interpreted in a similar way. The terms on the right hand side refer to the effects of detrainment, compensating subsidence and evaporation. The detrainment and evaporation tend to cause cooling and moistening whilst the subsidence results in warming and drying.

In order to compute s_u and χ_u, (5.1), (5.2) and (5.3) are manipulated to give

$$M_u \frac{\partial h_u}{\partial p} = 0 \tag{5.6}$$

$$M_u \frac{\partial s_u}{\partial p} = -\frac{L\bar{c}}{g} \tag{5.7}$$

$$M_u \frac{\partial \chi_u}{\partial p} = \frac{L\bar{c}}{g} \tag{5.8}$$

where $h_u = s_u + \chi_u$ is the moist static energy which is conserved in the plume (see (5.6)). Once h_u and M_u are known, (5.7) and (5.8) are integrated upwards from the base of the plume.

Let 0 and 1 refer to the base of the plume and the first level, and let Δp be the seperation of the levels. Writing (5.1) in finite difference form and rearranging yields

$$M_u' = \frac{(1 + \lambda \Delta p/2)}{(1 - \lambda \Delta p/2)} M_u^0$$

Since h_u is conserved we have

$$h_u' = h_u^0$$

To find χ_u' and s_u' we first set $\bar{c} = 0$ so that

$$s_u' = s_u^0 \qquad \chi_u' = \chi_u^0$$

Since the height of the first level is know (z' say), T_u' and r_u' are derived from

$$T_u' = \frac{s_u' - gz'}{c_p} \qquad r_u' = \frac{\chi_u'}{L}$$

If according to these calculations the plume is supersaturated at level 1, $r_u' > r_s(T_u')$, then we must allow some condensation to take place. Let $\tilde{T}_u'$ and $\tilde{r}_u' = r_s(\tilde{T}_u')$ be the temperature and mixing ratio after condensation has occured. Since h_u is still conserved $\tilde{T}_u'$ must satisfy

$$c_p \tilde{T}_u' + L r_s(\tilde{T}_u') = h_u' - gz'$$

The right hand side is known and the variation of r_s with temperature is given by the Clausius - Clapeyron equation, and so this equation can be solved for $\tilde{T}_u'$ using the Newton - Raphson method; the mixing ratio is then $r_s(\tilde{T}_u')$. The condensed water is assumed to be rain. This process is continued until the top of the plume is reached and the total condensation over the adjusted layers given the extra rainfall.

Rain may have to fall through an unsaturated part of the updraught before reaching the ground and so we allow evaporation to occur at a rate given by

$$\bar{e} = \alpha\gamma(r_s(T_u) - r_u)$$

where $\gamma = 10^{-3}\ s^{-1}$. It is necessary to use this, rather than the scheme used in the 10-level model, because we are dealing with only

the additional rainfall and evaporation. The total rainfall is now given by the rainfall from the 10-level model (convective and dynamic) plus the additional rainfall from the parameterisation scheme.

The horizontal velocity in the plume is assumed to satisfy an equation similar to that for h_u, so

$$\frac{\partial}{\partial p}(M_u \underline{V}_u) = \lambda M_u \underline{V}_u \qquad (5.9)$$

Using (5.1) this reduces to

$$M_u \frac{\partial \underline{V}_u}{\partial p} = 0$$

and so $\underline{V}_u$ is conserved in the plume. Using (5.1) and (5.9) in conjunction with (3.1) gives

$$\frac{\partial \bar{\underline{V}}}{\partial t} = g\lambda M_u(\underline{V}_u - \underline{V}_d) - g M_u \frac{\partial \underline{V}_d}{\partial p}$$

The values of h_u, s_u, χ_u and $\underline{V}_u$ at the bottom of the plume are taken to be the values at the topographic height which is already used in the 10-level model. The base value of M_u will be considered in the next section and the top of the plume is taken to be where M_u falls to 10% of its base value. The downdraught value of any variable θ is given by

$$\theta_d = \frac{\bar{\theta} - \alpha\theta_u}{1-\alpha}$$

where α, the fractional area of updraught, is taken to be 0.5

6. <u>The base value of M_u</u>

Suppose that in the direction of the wind the topography in a grid square has a cross-section of the kind shown in Figure 2, and that across the wind there is no variation in topography. Let there be Λ pairs of peaks and valleys, and let $4a$ be the distance from peak to peak. If h is a variable denoting the deviation of topography from its mean value (with a maximum value of t), then the standard deviation is given by

$$\sigma^2 = \frac{\int_0^d h^2 dx}{d}$$

where d is the gridlength. Between A and B in Figure 2, $h = \frac{tx}{a}$ with $a = d/4n$, so

$$s^2 = \int_0^a h^2 dx = \frac{t^2 a}{3}$$

There will be $4n$ similar contributions giving

$$\sigma^2 = \frac{4n s^2}{d} = \frac{t^2}{3} \qquad (6.1)$$

Whenever there is an upward gradient its value will be t/a and so the mean upward gradient over half the grid for the topography above the mean level is

$$G = \frac{1}{2n} \frac{t}{a} = \frac{2\sqrt{3}\sigma}{d} \qquad (6.2)$$

Hence the topography illustrated in Figure 2 can be replaced by a mean height plus a single peak of height $t = \sqrt{3}\sigma$.

The additional induced vertical velocity is

$$w_0 = V_0 G = V_0 \frac{2\sqrt{3}\sigma}{d} \qquad (6.3)$$

where V_0 is the horizontal velocity at the mean topographic height. The mass flux at the plume base then becomes

$$M_0 = \rho_0 \alpha w_0 = \rho_0 \alpha V_0 G \qquad (6.4)$$

In reality the topography does not have the form shown in Figure 2; however in the parameterisation scheme it is assumed that (6.1) and (6.2) always hold. Therefore the only extra parameter required is the standard deviation of the topography over the grid square.

The parameterisation scheme can easily be modified to take account of a grid square with both land and sea. Let β be the fraction of the gridsquare covered by land and let σ be the standard deviation of the land about its mean height. Using arguments similar to those above we find that

$$G = \frac{2\sqrt{3}}{d} \frac{\alpha}{\beta}$$

This is then used to compute M_0. The flux terms are also modified; for example (2.6) becomes

$$\overline{s'w'} = -\beta g M_u (s_u - s_d)$$

The additional topographic rain that falls over land is computed as before, but the grid mean value of now β times that amount.

7. The Choice of λ

In sections 4and 5 the detrainment rate λ was introduced and we now consider the form that λ should take. For typical values of V, k and f we find that $\sqrt{\frac{f^2}{V^2k^2} - 1} \approx 1$ so that (4.4) becomes

$$\lambda = \frac{l_0}{l_0 g} \tag{7.1}$$

Typically $l_0 \simeq 10^{-3}$ and so (7.1) gives a value of λ of about 10^{-2} mb^{-1} which corresponds to an e-folding distance of about 100 mb.

To a good approximation $l_0 = N_0/V_0$ (where N_0 is the Brunt-Vaisala frequency) and so it is probably sufficient to assume that λ is proportional to N_0/V_0 rather than use (4.4). Therefore we express λ in the form

$$\lambda = \left(\frac{V_c}{V_0}\right)\left(\frac{N_0}{N_c}\right)\hat{\lambda} \tag{7.2}$$

where V_c and N_c are typical values of V and N (here taken to be 10 ms^{-1} and 10^{-2}s^{-1}) which are used to non-dimensionalise N_0/V_0. The effects of using (7.1) will be discussed later.

8. The Choice of σ

Over the U.K. the topography is available on a $3\frac{1}{3}$ km grid and so the standard deviation of the topography for each grid square can be computed. However outside the U.K. detailed information about the topography is not so readily available and so it would be convenient if we could find some way of estimating σ.

The topography for each square in the U.K. was examined in terms of a non-dimensional height $s = (H - \bar{H})/D$ where H is the topographic

height, $\bar{H}$ its mean value and D is the difference between the maximum and minimum height. The frequency distribution for ζ was calculated along with its standard deviation σ_ζ (by definition $\bar{\zeta} = 0$). It was found that σ_ζ varied between 0.15 and 0.25 with a mean value of 0.2 Figure 3 shows the mean frequency distribution $q(\zeta)$ derived from the distribution for each of the grid squares; also shown is the gaussian distribution using $\sigma_\zeta = 0.2$. The similarity between the observed and suggested distributions is encouraging although naturally the gaussian distribution cannot reporduce the observed skewness; the skewness is due to the topography being characterised by broad areas of lowland and limited areas of relatively steep upland.

The relationship between the standard deviation of the topography and σ_ζ is

$$\sigma = \sigma_\zeta D \qquad (8.1)$$

Therefore if $\sigma_\zeta = 0.2$ is chosen we can estimate σ from a knowledge of D; it should be relatively easy to estimate D for each grid square.

The frequency distribution for the type of terrain discussed in section 6 is rectangular and is quite unlike that observed. However from (6.1) we find that $\sigma = D/2\sqrt{3}$ since $D = 2t$. Therefore, for the rectangular distribution we have $\sigma = 0.29\ D$ and this or similar to the relationship derived from the actual topography (see (8.1)).

9. Effects on $\bar{S}$ when no condensation occurs

It is interesting to examine the general effect on the large scale variables of parameterising the subgridscale topography.

Consider the dry static energy. If no condensation occurs $\bar{e} = 0$ and so (5.4) may be written as

$$\frac{\partial \bar{S}}{\partial t} = F_1 + F_2 = F$$

where F_1 and F_2 are the effects of detrainment and compensating subsidence. We now assume that $\bar{S}$ varies linearly with pressure, so

$$\bar{S} = S_0 + \alpha(p_0 - p)$$

where S_0 is the value of $\bar{S}$ at the mean topographic height (corresponding to a pressure p_0). Since we have assumed that $\bar{e} = 0$

$$S_u = S_0 \qquad S_d = \frac{\bar{S} - \alpha S_u}{1-\alpha} \tag{9.2}$$

The mass flux is computed from (5.1) giving

$$M_u = M_0 \exp\{\lambda(p-p_0)\} = M_0 f \tag{9.3}$$

Using (9.1), (9.2) and (9.3) yields

$$\frac{1}{gM_0a} F_1 = -\frac{f(p_0-p)\lambda}{(1-\alpha)}$$

$$\frac{1}{gM_0a} F_2 = \frac{f}{(1-\alpha)}$$

$$\frac{1}{gM_0a} F = f\left\{\frac{1-\lambda(p_0-p)}{1-\alpha}\right\} \tag{9.4}$$

Figure 4a shows F_1, F_2 and F in units of gM_0a as a function of (p_0-p). The effects of detrainment and subsidence are in the opposite sense and this leads to a reversal of the sign of $\frac{\partial \bar{S}}{\partial t}$ at about 800 mb.

It is necessary to interpret $\frac{\partial \bar{S}}{\partial t}$ in terms of the rate of change of temperature $\frac{\partial \bar{T}}{\partial t}$. Usually $g\frac{\partial z}{\partial t}$ is neglected when compared with $c_p \frac{\partial \bar{T}}{\partial t}$ so that

$$\frac{\partial \bar{T}}{\partial t} = \frac{1}{c_p}\frac{\partial \bar{S}}{\partial t} \tag{9.5}$$

An alternative procedure is to use a differential equation for $\frac{\partial \bar{T}}{\partial t}$, namely

$$c_p \frac{\partial}{\partial p}\frac{\partial \bar{T}}{\partial t} - g\frac{\partial}{\partial t}\frac{\partial z}{\partial p} = \frac{\partial}{\partial p}\frac{\partial \bar{S}}{\partial t}$$

Using the hydrostatic equation this becomes

$$c_p \frac{\partial}{\partial p}\frac{\partial \bar{T}}{\partial t} - R\frac{\partial \bar{T}}{\partial t} = \frac{\partial}{\partial p}\frac{\partial \bar{S}}{\partial t}$$

where R is the gas constant. The right hand side is known and by

setting $\frac{\partial \bar{T}}{\partial t} = 0$ at the top of the atmosphere the equation can then be integrated downwards. This procedure was tested and found to give almost the same results at (9.5); in the following calculations (9.5) was used.

Figure 4a shows that the maximum heating occurs at $p = p_0$, and using (6.4), (9.4) and (9.5) this is given by

$$\frac{\partial \bar{T}}{\partial t} = \frac{\rho_0 g V_0}{c_p} \frac{a}{d} 2\sqrt{3}\sigma \qquad (9.6)$$

A reasonable value of a is 0.44 and using $V_0 = 5\ ms^{-1}$, $\alpha = 0.5$, $d = 10^5 m$ and $\sigma = 150\ m$ yields a maximum warming of 11.6°C/day (this is independent of λ).

It is interesting the compare the heating effects of the gridscale and subgridscale processes. If there is a difference in mean topographic height between adjacent grid squares ($\Delta\bar{H}$ say), then the induced vertical velocity is $\omega_E = \rho_0 g V_0 \frac{\Delta \bar{H}}{d}$ and the resulting rate of change of temperature is given by

$$\frac{\partial \bar{T}}{\partial t} = -\omega_E \frac{\partial \bar{S}}{\partial p} = -\frac{\rho_0 g V_0}{c_p} \frac{a}{d} \Delta \bar{H} \qquad (9.7)$$

Comparison of (9.6) and (9.7) shows that when the air is flowing up the gridscale topography ($\Delta \bar{H} > 0$) the contributions to the temperature tendency from the gridscale and subgridscale effects are in the opposite sense; for flow down the gridscale topography ($\Delta \bar{H} < 0$) both contributions produce a warming.

The ratio of the temperature changes due to the subgridscale and gridscale topography is $2\sqrt{3}\sigma / \Delta \bar{H}$. Typically $\Delta \bar{H}$ is in the range σ to 2σ and so the magnitude of the effects due to subgridscale topography are of the order of 1.5 to 3.5 times those due to the gridscale topography. Assuming this is a realistic estimate then the subgridscale effects can be considerable.

10. Effects on the large scale variables when condensation occurs

Once again we consider the dry static energy. As in the previous section $M_u = M_0 f$ and we assume that $\bar{c} = c_0 f$ so that (5.7) becomes

$$\frac{\partial s_u}{\partial p} = \frac{-Lc_0}{gM_0} \qquad (10.1)$$

where c_0 is the condensation rate at the base of the plume. Since $s_u(p_0) = s_0$, the integration of (10.1) yields

$$s_u = s_0 + \frac{Lc_0}{gM_0}(p_0 - p)$$

As expected $s_u > s_0$ when condensation occurs ($c_0 > 0$) because of the release of latent heat. Following the procedure in the previous section we find that

$$\frac{1}{gM_0 a}\frac{\partial \bar{s}}{\partial t} = f\left\{\frac{1-\lambda(p_0-p)}{1-\alpha}\right\} + \delta$$

with

$$\delta = \frac{Lc_0 f}{gM_0 a}\left\{\frac{\lambda(p_0-p)-\alpha}{1-\alpha}\right\} \qquad (10.2)$$

Here δ represents the combined effects due to condensation; when $c_0 = 0$ (10.2) reduces to (9.4). Since c_0 is likely to be proportional to M_0 we use

$$c_0 = 1.6\times10^{-2} M_0$$

The rainfall rate is found by integrating c throughout the plume, so that

$$R = 3.6\times10^{5}\frac{c_0}{\lambda g}(1-e^{-\lambda p_0}) \quad \text{mm/hr}$$

With $\lambda = 6\times10^{-3}$ mb^{-1} amd $M_0 = 0.016$ kg m^{-2}s^{-1} (computed from V_0, α, d and σ given earlier) we have R = 0.15 mm/hr. Although this may appear a comparitively small rainfall rate it will increase with V_0 and on some occasions we might expect this additional rain to make a significant contribution to the forecast rainfall.

Figure 4b shows $\frac{\partial \bar{T}}{\partial t}$ with and without condensation; when condensation occurs there is a general warming throughout the column, although this is only really significent in the first few hundred millibars above the topography. Also one of the effects of condensation is to decrease the maximum warming from about 11°C/day to 6°C/day. This comes about because the release of latent heat increases S_u, and the resulting increase in cooling due to detrainment is greater than the increase due to subsidence.

A similar analysis can be carried out for water vapour (in terms of $\chi = L r$). With $\chi = \chi_0 + a(p_0 - p)$ a suitable value of a is - 0.22. If no condensation occurs we find that there is drying below 800 mb and moistening above, and that the maximum drying is 2.4 gn/kg/day (corresponds to a cooling of 6.0°C/day). When condensation occurs the distribution of drying and moistening is unchanged, but there is an increase in the maximum drying to 11.2°C/day.

When real data was used we found that the magnitude and sign of the effects on the large scale were similar to those described above. For example, measured in °C/day, the maximum drying was usually about twice the magnitude of the maximum warming. The significant drying and warming of the air just above the topography should lead to a marked decrease in the relative himidity and this may have important effects downstream.

For momentum a reasonable value for a is 0.16×10^{-3} and this produces a maximum increase in momentum of 4.3 ms^{-1}/day.

11. The data

The basic data consisted of hourly values of large scale fields from the rectangle version of the 10-level model. Forecasts based on midnight data were made for 14 consecutive days; the same data was used by B. The tests used forecast fields between T+9 and T+33 which concides with a rainfall day. Ultimately two forecasts were rejected due to the poor

quality of the basic rectangle forecast (5th and 16th October 1976).

The ability of the parameterisation scheme to forecast rainfall in rough terrain was tested over the same area as was used by B ; the topography is shown in Figure 5. Although the rainfall was computed in all 12 grid squares, the verification was only performed on the squares marked 1 to 4. Table 1 shows $\bar{H}$, σ and D for the verification squares.

The 24 hr. rainfall accumulation was the main quantity used for comparison purposes, comparisons being made between

i. the raingauge estimates

ii. the 10-level model rainfall

iii. the rainfall from Bell's orographic model

iv. the rainfall from the parameterisation scheme plus that from the 10-level model.

When rainfall accumulation statistics are computed the results from the 4 areas will be assumed independent so that there are 48 independent results.

Figures 6a and 6b show scatter diagrams of (i) against (ii) and (i) against (iii). These indicate that both (ii) and (iii) underestimate the rainfall, but that overall (iii) is probably the better of the two models. This is also illustrated by the 12 day accumulations shown in Table 2. Using a t-test we find that the use of (iii) instead of (ii) to calculate rainfall accumulation produces a highly significant improvement; B came to the same conclusion. Therefore Bell's model has a large amount of skill in predicting rainfall accumulations.

Since there is a large scatter when results from models are compared with rainguage estimates it is convenient to concentrate on comparisons between the parameterisation scheme and Bell's model. This approach has been adopted in the following experiments.

12. Some experiments

So far experiments have only been carried out with a non-interactive version of the parameterisation scheme.

Experiments were carried out with λ ranging from 4×10^{-3} to 8×10^{-3} mb^{-1}

(corresponding to an e- folding distance of 250 mb to 125 mb). The 12 day rainfall accumulations are shown in Table 2, and Table 3 has the correlation coefficients with respect to Bell's model and the raingauge estimates. Table 3 also has the coefficients of the regression equation which relates the 24 hr accumulations from the parameterisation scheme (A_p say) with those from Bells model (A_b say), so that

$$A_p = a + b A_b$$

Ideally we would like $a = 0$ and $b = 1$; Table 3 shows that this never happens. In fact as λ increases a approaches 0, but as λ decreases b approaches 1. Also Table 2 shows that as λ increases the total accumulated rainfall decreases.

Figures 7, 8 and 9 are scatter diagrams for 3 values of λ. Figure 7a shows that $\lambda = 4 \times 10^{-3}$ produces accumulations that are nearly all in excess of those from Bell's model, and this is also reflected in Table 2. The use of $\lambda = 6 \times 10^{-3}$ produces no general bias, but there is a tendency for small rainfall accumulations to be overestimated (see Figure 8); the 12 day accumulations are similar to those for Bell's model. Figure 9 shows that the use of $\lambda = 8 \times 10^{-3}$ tends to underestimate the accumulations and that the small accumulations are treated better than when $\lambda = 6 \times 10^{-3}$. Overall $\lambda = 6 \times 10^{-3}$ appears a reasonable compromise value, although there must be some concern about the overestimate of small accumulations.

We now consider comparisons with the raingauge estimates. Figures 6a, 6b and 8b show scatter diagrams of various predicted accumulations against the raingauge estimates. Also shown are the regression equations and correlation coefficients. These results emphasise the superiority of both the Bell model and the parameterisation scheme over the 10-level model alone. This is confirmed by a t-test. Also we find that there is no significant difference in the accumulations from Bell's model and the parameterisation scheme.

The effects of including a wind speed and stability dependence for λ were considered (see section 8). Tables 2 and 3 show the results

of using (7.2) with $\hat{\lambda} = 6\times10^{-3}$, $V_c = 10\ ms^{-1}$ and $N_c = 10^{-2}s^{-1}$. Several combinations were tried and in all cases the results were essentially the same as when $\lambda = 6\times10^{-3}$ was used.

Another experiment was performed with λ given by (7.1). The results are given in Figure 10 and these show a remarkable similarity to those for $\lambda = 8\times10^{-3}$ (see Figure 9). Again these results indicate that there is little point including a wind or stability dependence for λ.

In section 8 a method of estimating σ from $D=H_{max} - H_{min}$ was discussed. To test this computations were carried out with $\lambda = 6\times10^{-3}$ and σ given by (8.1). D was calculated from the $3\frac{1}{3}$ km orography data. The results are shown in Figure 11 and comparison with those using the actual σ (Figure 8) reveals that the estimated σ gives surprisingly good results. Further tests are required to show if (8.1) is generally valid.

So far only accumulations have been considered and so we now compare the hourly rainfall rates derived from the parameterisation scheme and Bell's model. Each of the four regions is considered separately and so there are 288 sets of rainfall rates per region. Figures 12 and 13 show the results for $\lambda = 6\times10^{-3}$ using the observed σ. (These rainfall rates correspond to the accumulations shown in Figure 8). Regions 2 and 4 have a comparitively small σ and in both cases the rainfall rates from the two models are highly correlated with little bias. The results from region 1 indicate a tendency for the parameterisation scheme to overestimate small rainfall rates, but for higher rainfall rates the results are similar to those from Bell's model. Region 3 is the most mountainous and represents a severe test for the parameterisation scheme. The results show that the largest rainfall rates are underestimated by the parameterisation scheme and that on many occassions it forecast small amounts of rain when Bell's model produced none. This behaviour is illustrated by Figure 14 which

shows the variation of rainfall rate throughout day 3 (3rd October) for regions 1 and 3. In both regions the parameterisation scheme tends to underestimate the large rainfall rates during the early part of the forecast, but overestimates the small rates which occur later.

Comparisons of the rainfall rates from the 10-level model and Bell's model show a marked tendency for the 10-level model to underestimate the rainfall rates in all the regions all the time.

12. Conclusions

These experiments have shown that the 24 hr accumulations of rainfall from the parameterisation scheme are highly correlated with those from Bell's orographic model and that there is no significant difference between the two sets of accumulations. The correspondence between the two schemes is surprising since Bell's model uses 900 extra pieces of information for each 100 km square (the topography on a $3\frac{1}{3}$ km grid) whereas the parameterisation scheme uses only one (the standard deviation of the topography). The parameterisation scheme produces significantly better forecasts of rainfall accumulations than the 10-level model alone.

The main defect of the parameterisation scheme is its tendency to overestimate small rainfall rates in mountainous regions and to produce small amounts of rain when there should be none. This effect can be reduced by increasing λ, but this would lead to a more pronounced underestimate of the large rainfalls.

The parameterisation scheme and Bell's model are now undergoing a more extensive test to ascertain their usefulness over the whole of the U.K. Also it is hoped to test the parameterisation scheme by incorporating it into a numerical model so that it can be used in its interactive mode.

References

Bates,J.R. 1977 "Parameterisation of convective process" Seminars 1977, E.C.M.W.F.

Bell,R.S. 1978 "The forecasting of orographically enchanced rainfall accumulations using 10-level model data" Met.Mag.,107,113-124.

Eliassen,A. 1973 "Airflow over mountains" Summer School 1973 on Mesoscale Meteorological Phenomena, National Research Council, Italy.

Schneider,E. and R.S.Lindzen 1976 "A discussion of the parameterisation of momentum exchange by cumulus convection" J.Geophys.Rev.,81,3158-3160.

White,P.W. 1972 "Fronts and small scale orographic effects" Report of the JOC Study Group Conference in Leningrad, 20-27 March 1972, Garp Publication Series No.8.

Wickham,P.G. 1977 "Errors in rainfall forecasts by the 10-level model 1973-1977" Met O 11 Tech.Note No.99.

	$\bar{H}$	σ	D
1	148	108	656
2	111	37	246
3	271	123	613
4	113	54	345

Table 1 - Mean height ($\bar{H}$), standard deviation (σ) and the difference between maximum and minimum heights (D) for the 4 verification grid squares; all heights are in metres.

	Region				
	1	2	3	4	Average
Raingauge estimate	59	46	79	52	59
Bell's model	37	22	70	30	40
10-level model	16	12	19	17	16
$\lambda = 4 \times 10^{-3}$	60	26	89	37	53
$\lambda = 5 \times 10^{-3}$	51	23	76	33	46
$\lambda = 6 \times 10^{-3}$	45	21	65	30	40
$\lambda = 7 \times 10^{-3}$	40	19	56	27	36
$\lambda = 8 \times 10^{-3}$	36	18	51	25	33
$\lambda = 6 \times 10^{-3}$, $\sigma = 0.2D$	51	37	54	47	47
$\lambda = l_0 / l_{0g}$	36	18	50	25	32
$\lambda = 6 \times 10^{-3}$	45	21	65	30	40
$\lambda = 6 \times 10^{-3} \left(\frac{V_c}{V_0}\right)$	47	22	66	30	41
$\lambda = 6 \times 10^{-3} \left(\frac{V_c}{V_0}\right)\left(\frac{N_0}{N_c}\right)$	47	22	67	30	41

Table 2 - 12 day accumulations of rainfall in mm from different models.

	correlation coeff.		Regression Equation	
	with Bells Model	with Raingauge estimate	a	b
10-level model	0.84	0.51	-0.48	0.54
$\lambda = 4\times10^{-3}$	0.90	0.50	1.35	0.92
$\lambda = 5\times10^{-3}$	0.92	0.51	1.00	0.85
$\lambda = 6\times10^{-3}$	0.93	0.52	0.71	0.79
$\lambda = 7\times10^{-3}$	0.93	0.53	0.47	0.75
$\lambda = 8\times10^{-3}$	0.93	0.53	0.34	0.72
$\lambda = 6\times10^{-3}$, $\sigma = 0.2D$	0.87	0.47	1.60	0.70
$\lambda = l_0 / C_0 g$	0.90	0.48	0.33	0.71
$\lambda = 6\times10^{-3}$	0.93	0.52		
$\lambda = 6\times10^{-3}(V_0/V_0)$	0.87	0.46		
$\lambda = 6\times10^{-3}(V_0/V_0)(W_0/W)$	0.86	0.44		

Table

Figure 3 - correlation coefficients between 24 hr. accumulations from various versions of the parameterisation scheme and both Bell's model and the raingauge estimates; also the coefficients of the linear regression equation relating the accumulations from the parameterisation scheme to those from Bell's model.

LIST OF FIGURES

Figure 12 Scatter diagrams of hourly rain rates (mm/hr) from the parameterisation scheme and orographic model for (a) region 1 and (b) region 3.

Figure 13 Hourly rain rates for (a) region 2 and (b) region 4.

Figure 14 Variation of rain rate with time for 3/10/76 for (a) region 1 and (b) region 3.

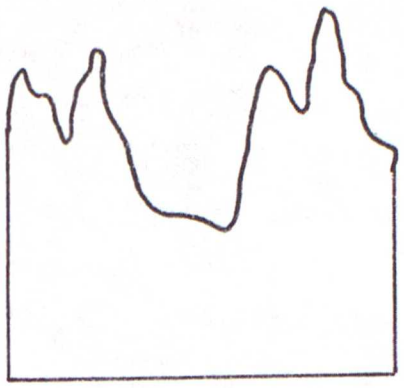

(a) actual

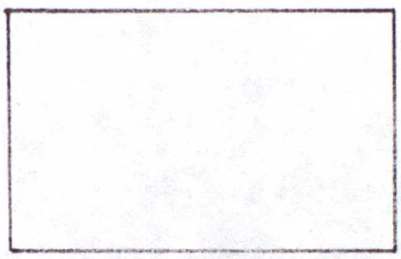

(b) 10-level model

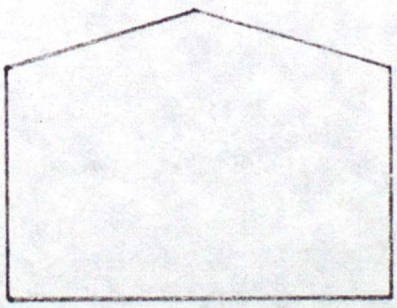

(c) parameterisation scheme

Figure 1

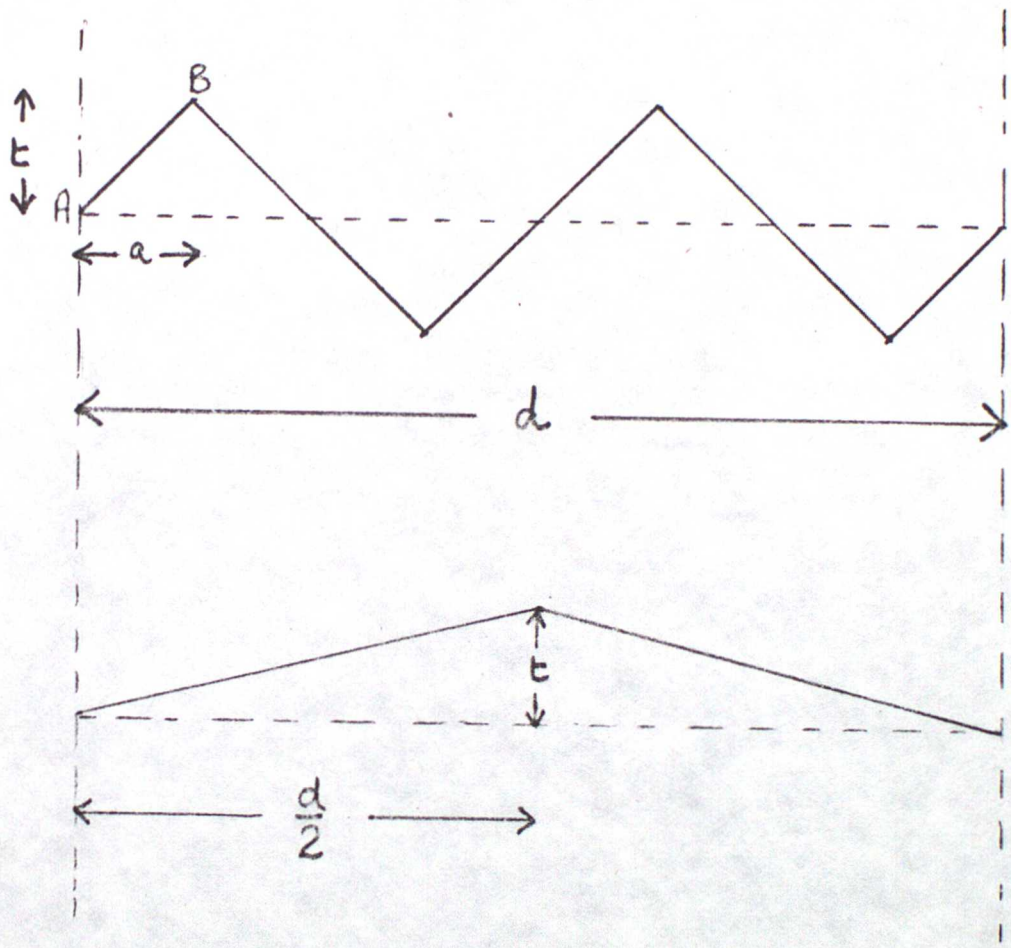

Figure 2

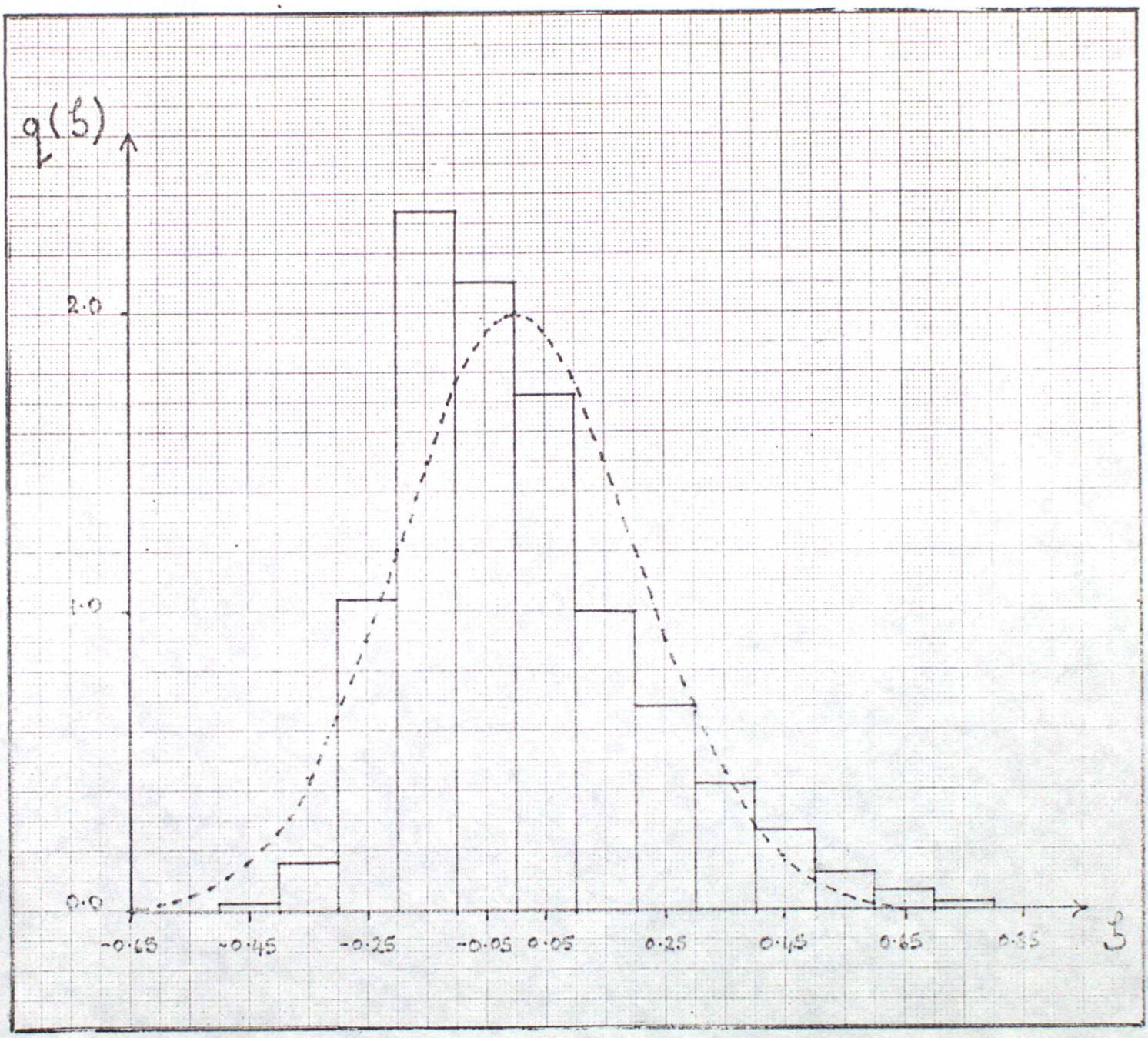

Figure 3

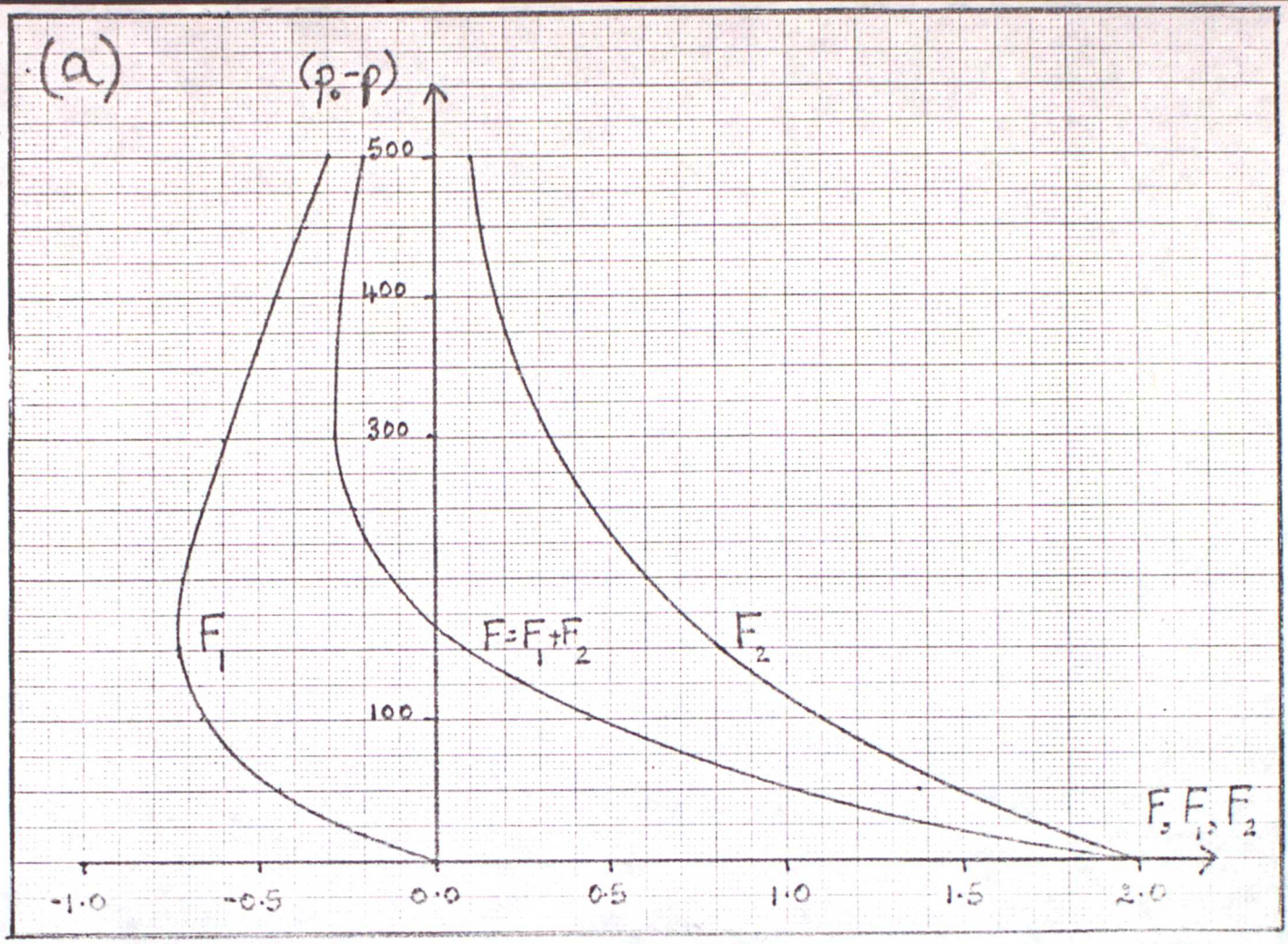
(a)
(p_0-p)
500
400
300
100
F_1
$F=F_1+F_2$
F_2
F, F_1, F_2
-1·0
-0·5
0·0
0·5
1·0
1·5
2·0

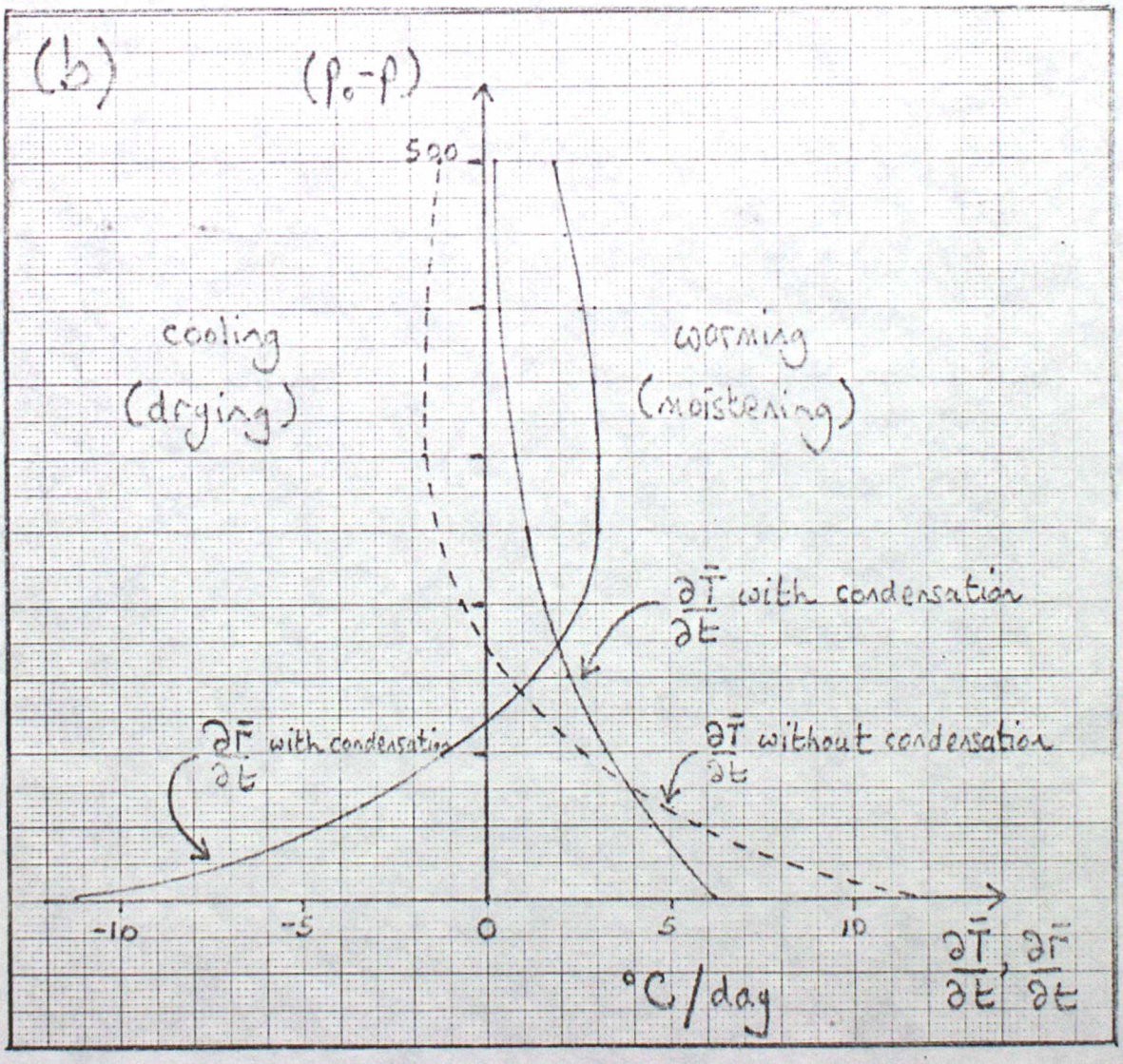
(b)
(p_0-p)
500
cooling
(drying)
warming
(moistening)
$\frac{\partial \bar{T}}{\partial t}$ with condensation
$\frac{\partial \bar{r}}{\partial t}$ with condensation
$\frac{\partial \bar{T}}{\partial t}$ without condensation
-10
-5
0
5
10
°C/day
$\frac{\partial \bar{T}}{\partial t}, \frac{\partial \bar{r}}{\partial t}$

Figure 4

Figure 5

(a.)

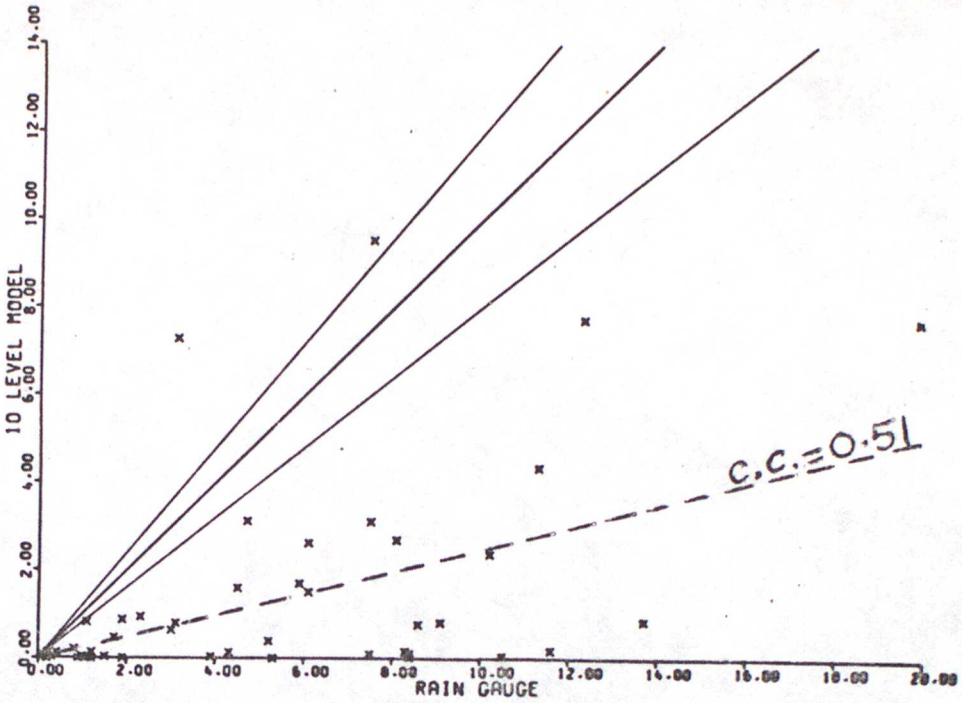

24 HR RAIN ACCUMULATIONS (MM)

(b)

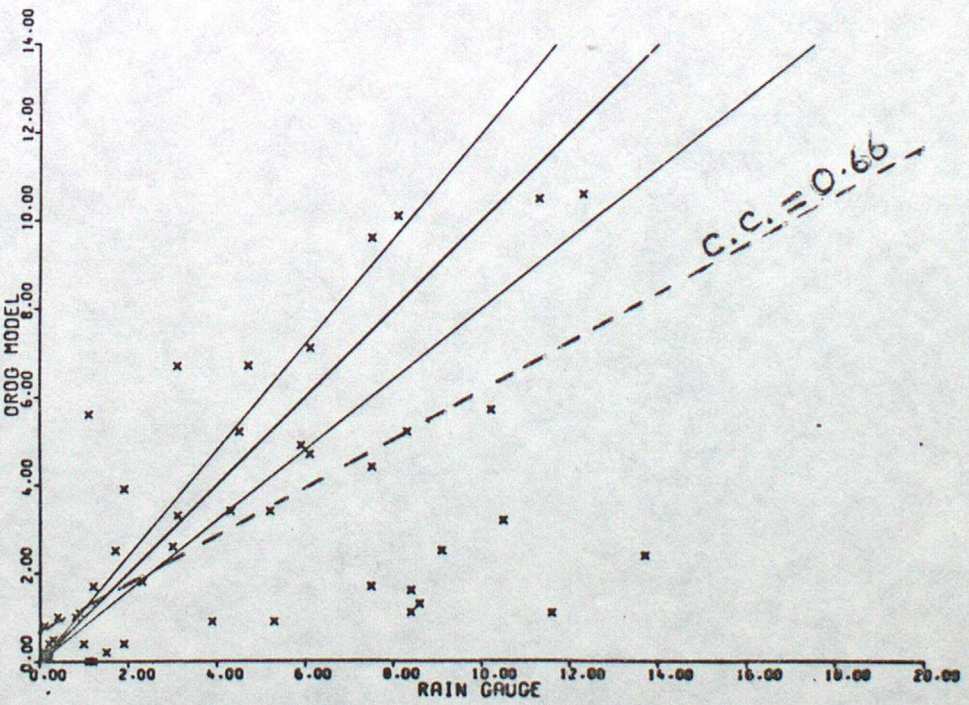

24 HR RAIN ACCUMULATIONS (MM)

Figure 6

(a)

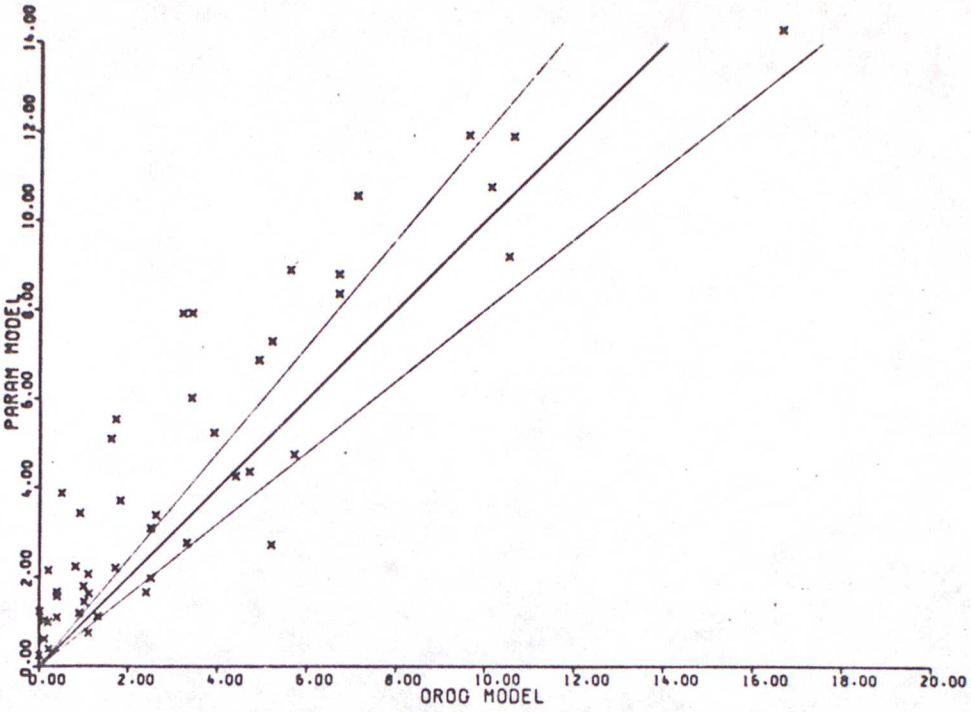

24 HR RAIN ACCUMULATIONS (MM)

(b)

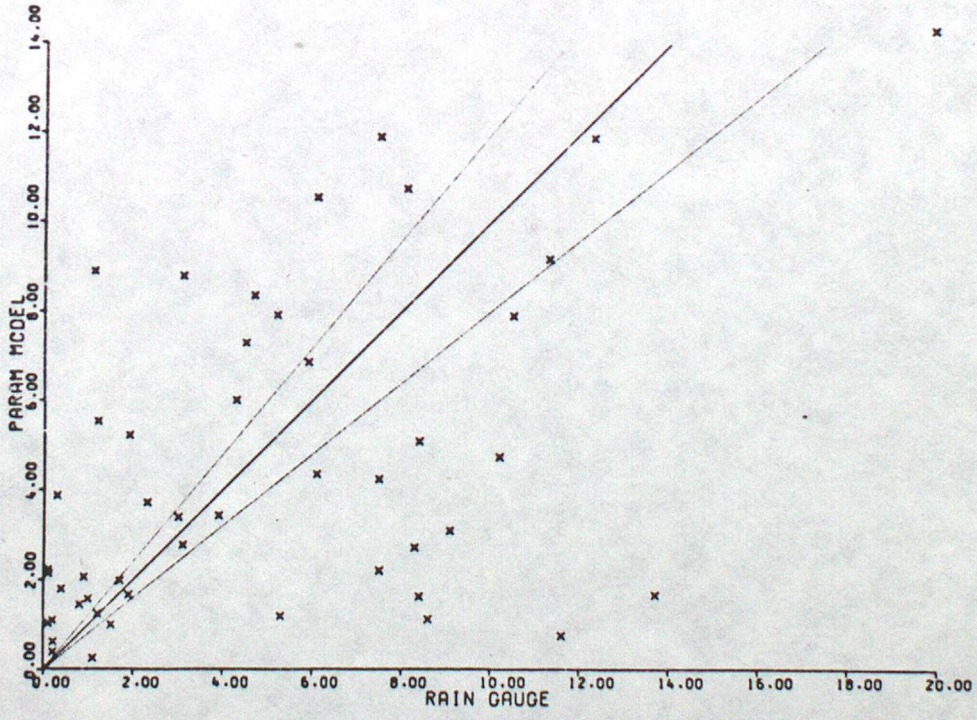

24 HR RAIN ACCUMULATIONS (MM)

Figure 7

(c)

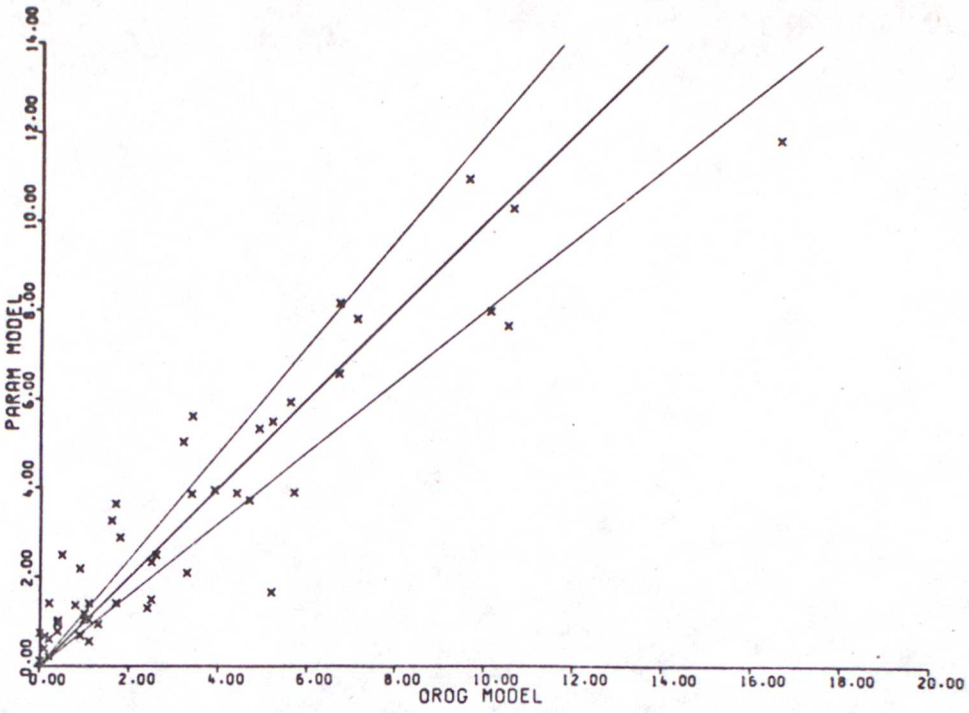

24 HR RAIN ACCUMULATIONS (MM)

(b)

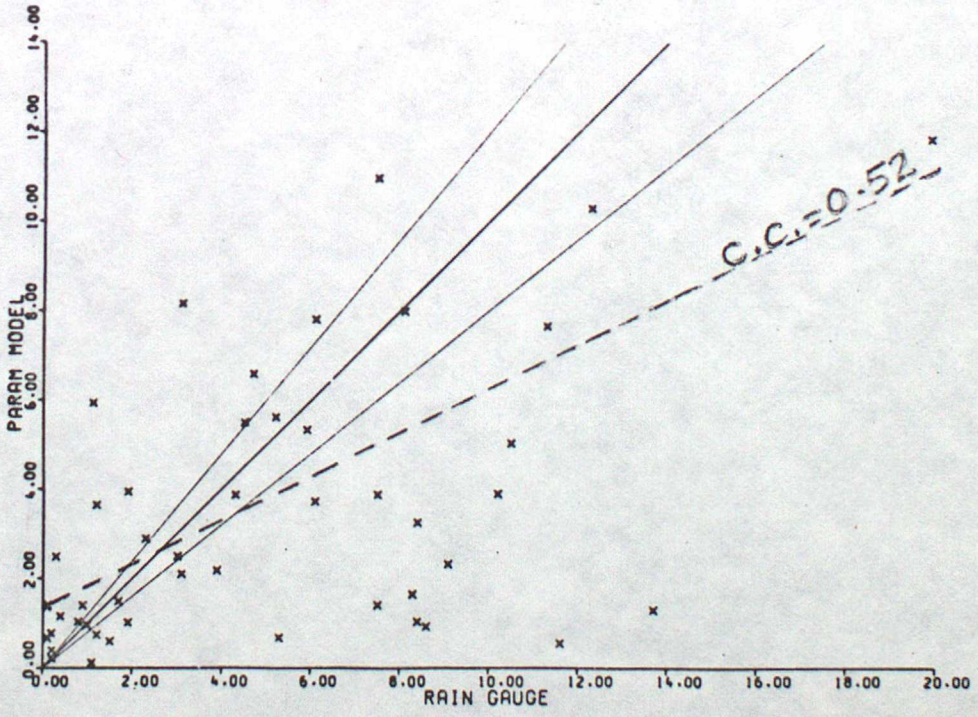

24 HR RAIN ACCUMULATIONS (MM)

Figure 8

(a)

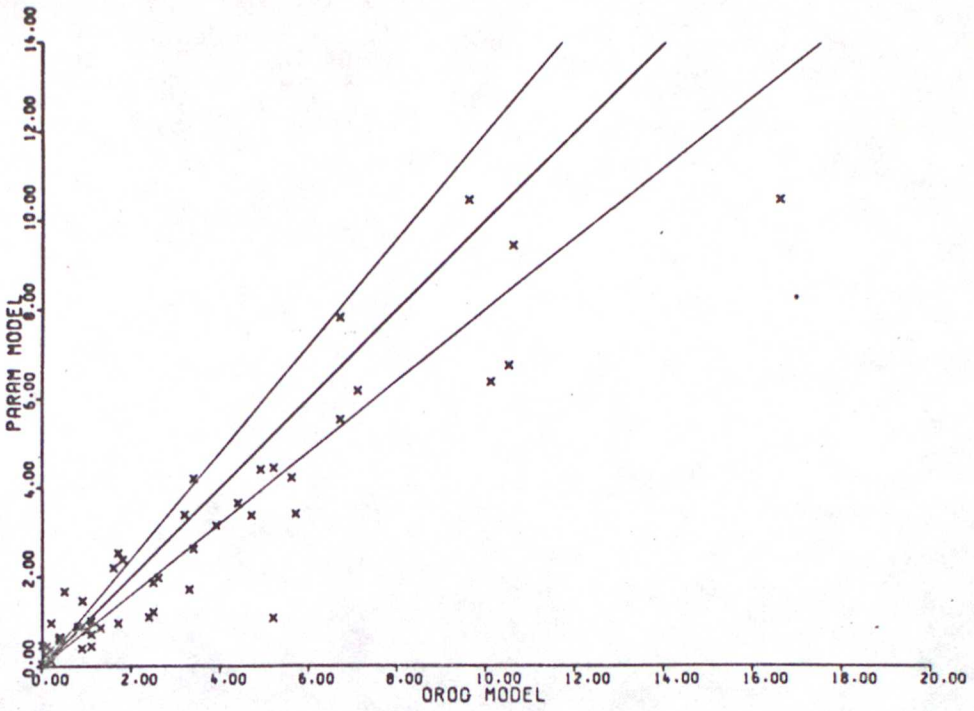

24 HR RAIN ACCUMULATIONS (MM)

(b)

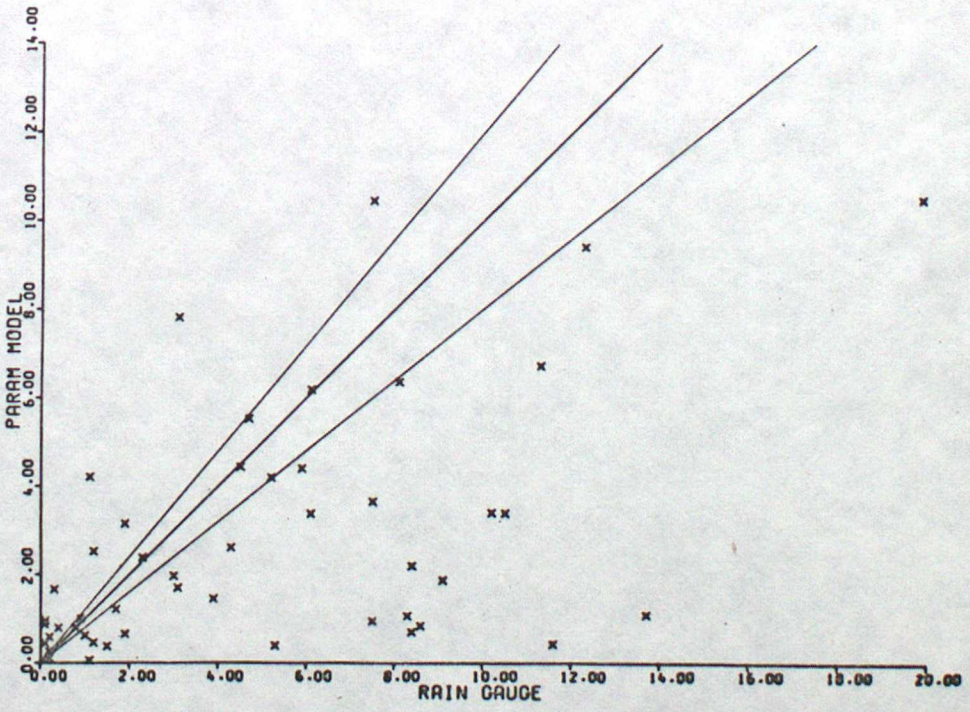

24 HR RAIN ACCUMULATIONS (MM)

Figure 9

(a)

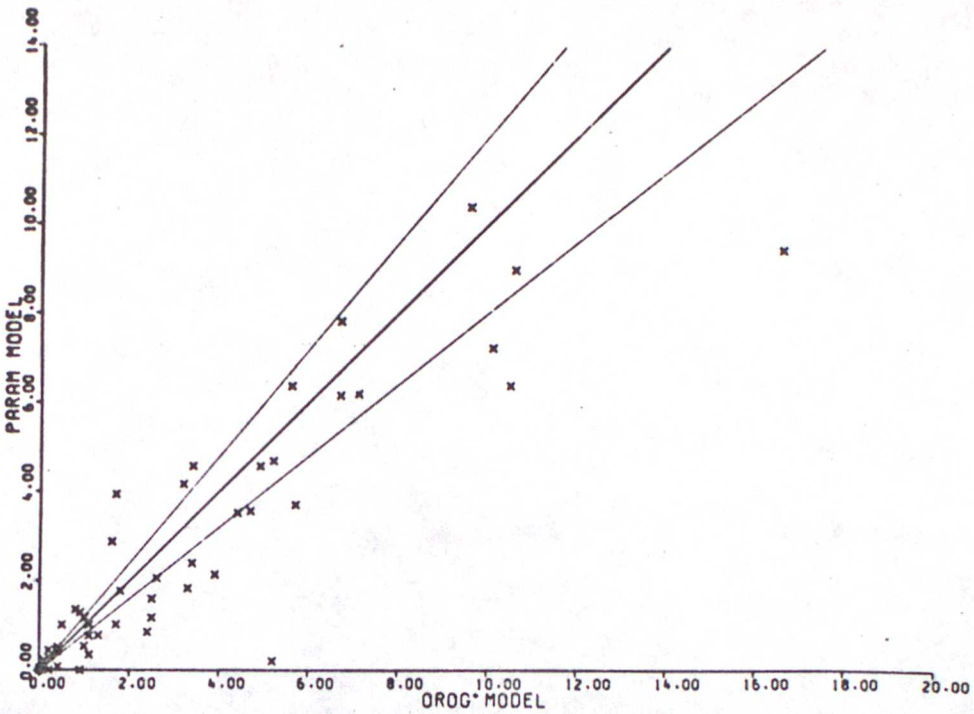

24 HR RAIN ACCUMULATIONS (MM)

(b)

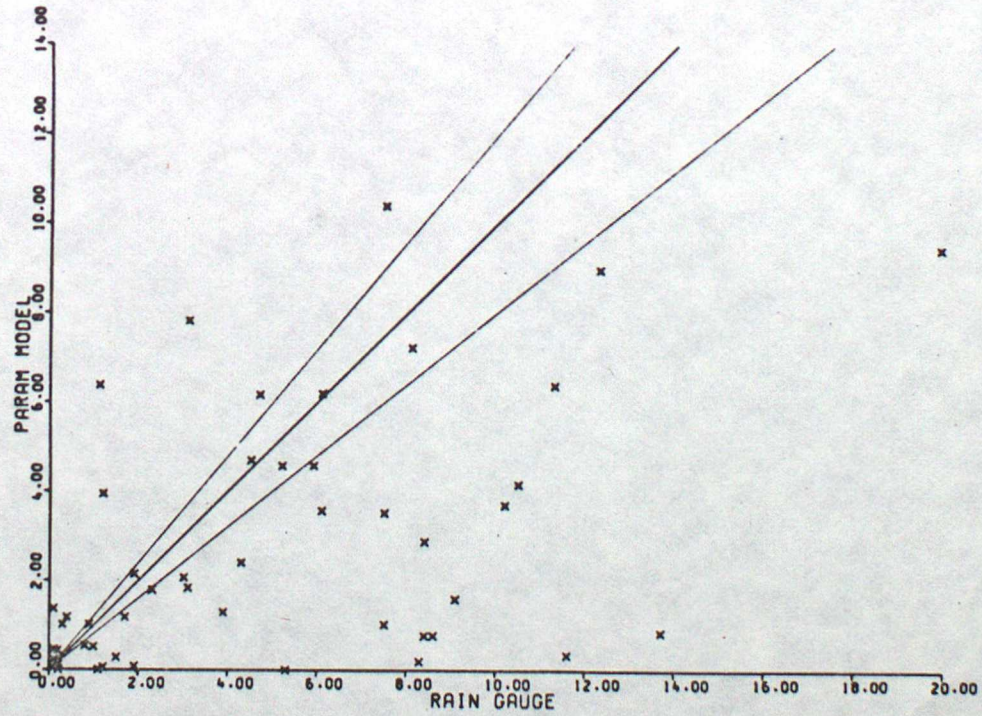

24 HR RAIN ACCUMULATIONS (MM)

Figure 10

(a)

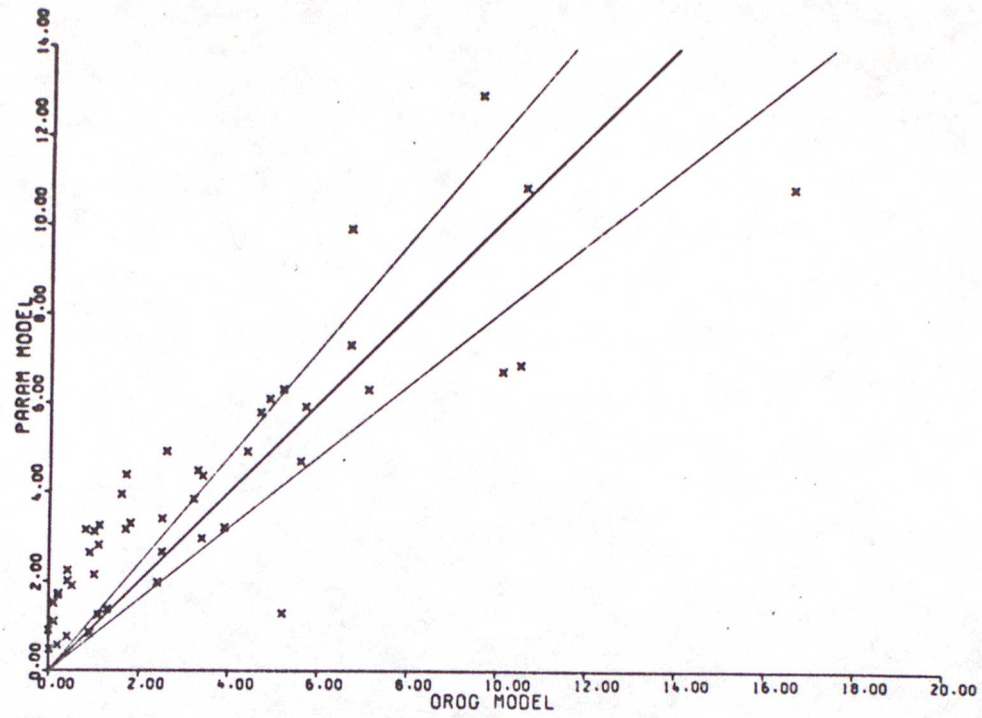

24 HR RAIN ACCUMULATIONS (MM)

(b)

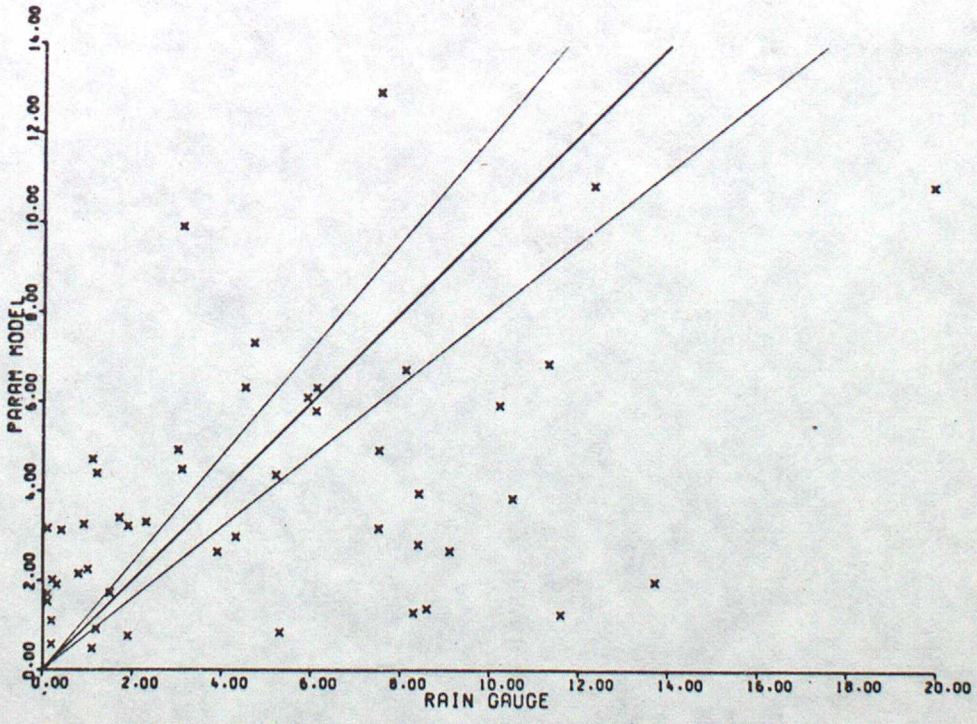

24 HR RAIN ACCUMULATIONS (MM)

Figure 11

(c)

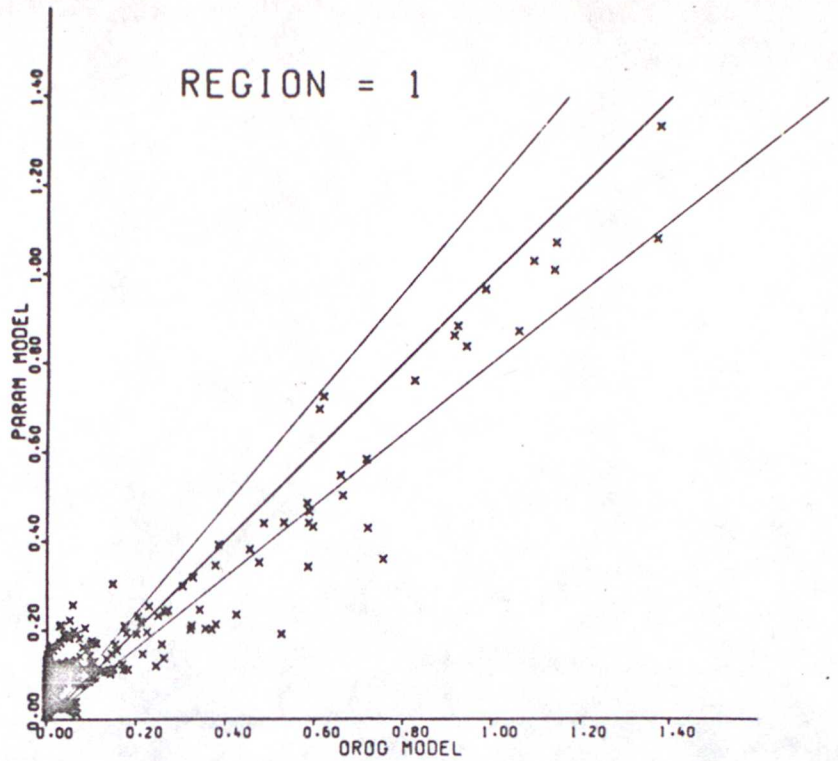
REGION = 1
PARAM MODEL
0.00
0.20
0.40
0.60
0.80
1.00
1.20
1.40
OROG MODEL
HOURLY RAIN RATE (MM/HR)

(b)

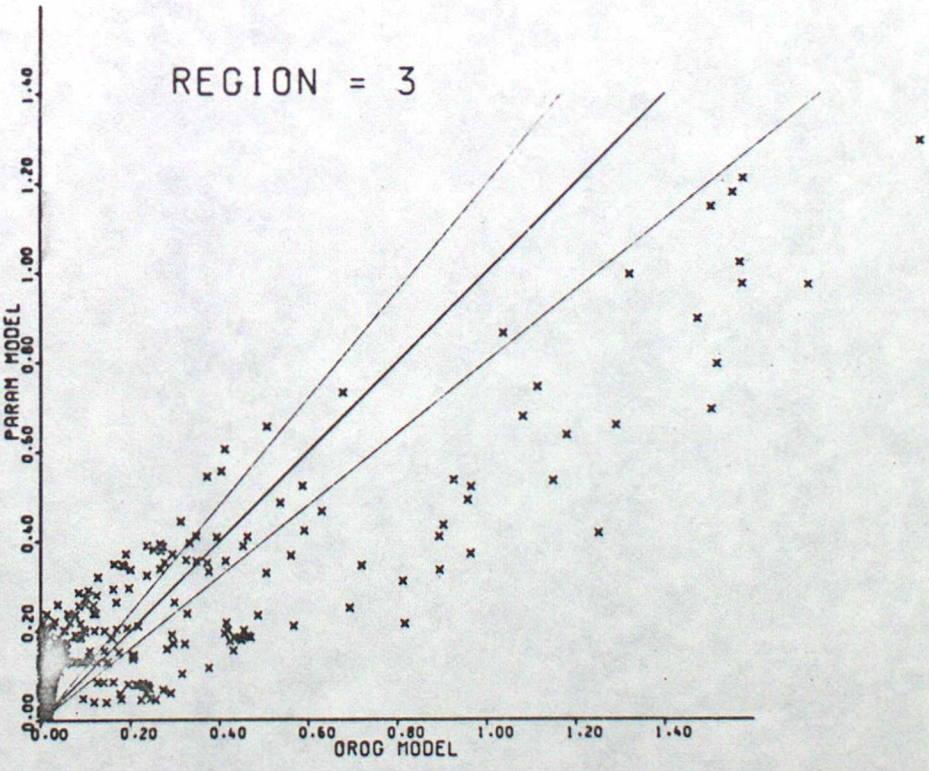
REGION = 3
PARAM MODEL
0.00
0.20
0.40
0.60
0.80
1.00
1.20
1.40
OROG MODEL
HOURLY RAIN RATE (MM/HR)

Figure 12

(a)

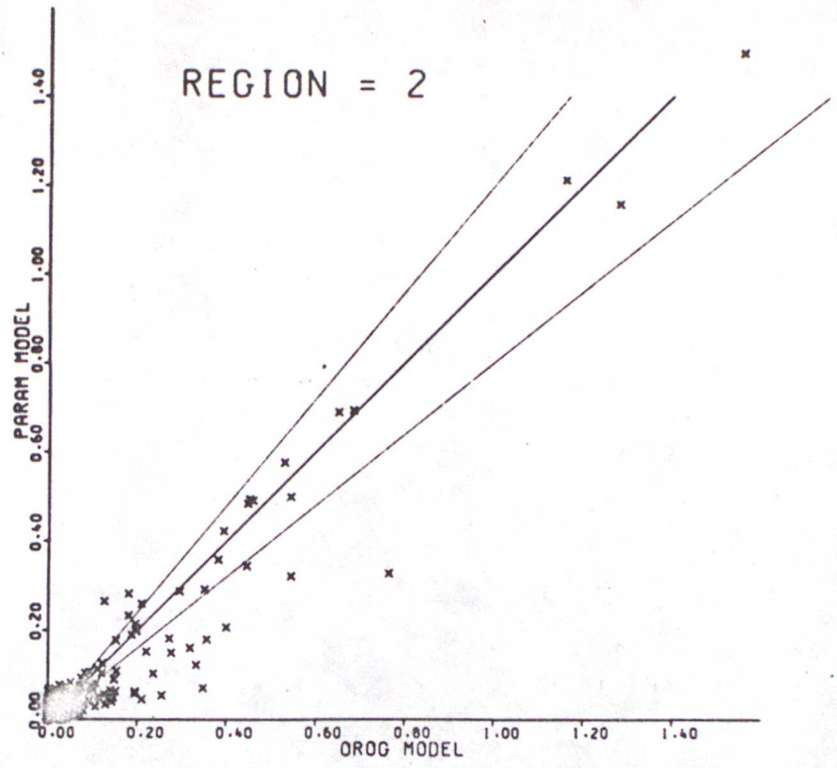
REGION = 2
PARAM MODEL
0.00
0.20
0.40
0.60
0.80
1.00
1.20
1.40
OROG MODEL
HOURLY RAIN RATE (MM/HR)

(b)

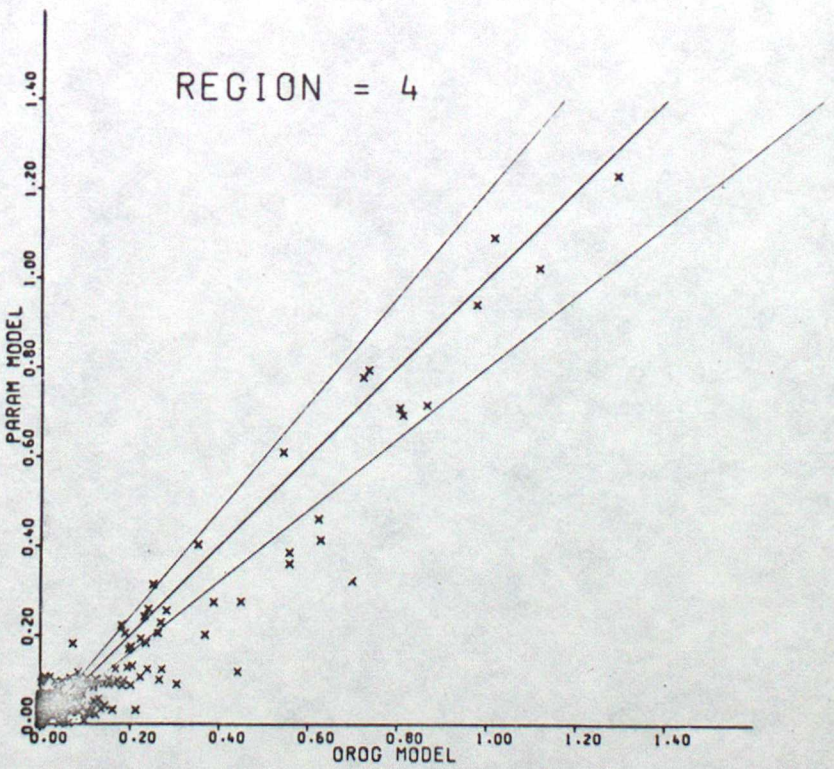
REGION = 4
PARAM MODEL
0.00
0.20
0.40
0.60
0.80
1.00
1.20
1.40
OROG MODEL
HOURLY RAIN RATE (MM/HR)

Figure 13

(a)

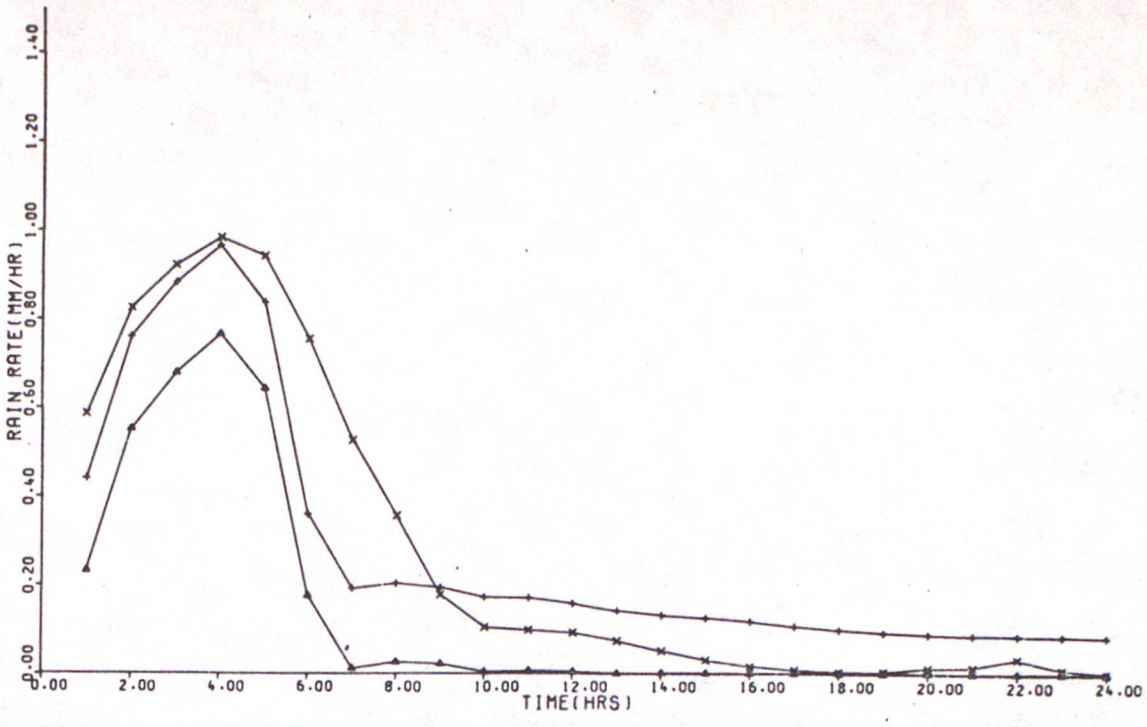

RAIN RATE/TIME DAY=3 REGION=1

(b)

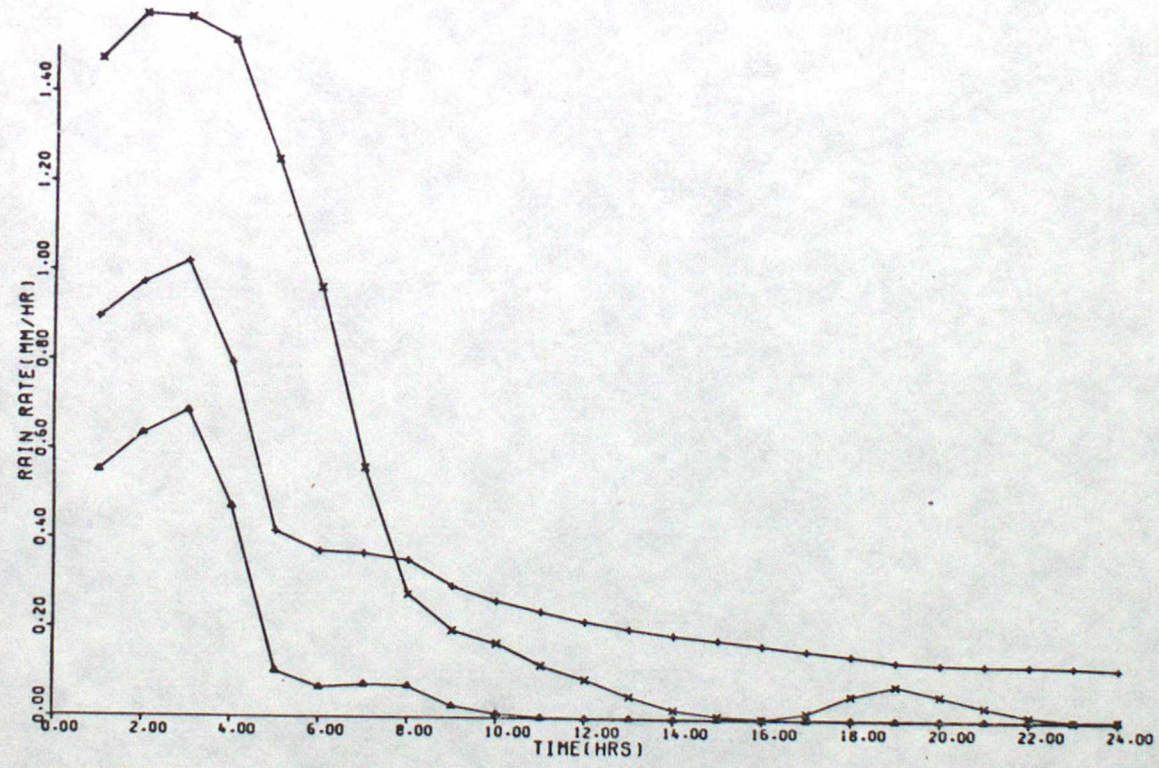

RAIN RATE/TIME DAY=3 REGION=3

△ - 10 LEVEL MODEL

\+ - PARAM MODEL

× - OROG MODEL

Figure 14